Electronic Supplementary Material (ESI) for Sustainable Energy & Fuels.

ELECTRONIC SUPPLEMENTARY INFORMATION (ESI)

Title: Multiferroic $BiFeO_3$ Based Hydrophobic Polymer Composites for Polarization Rationalization Induced Piezo-Tribo Hybrid Energy Harvesting and Versatile Self-Powered Mechanosensing

Abhishek Sasmal[a], Aniket Patra[b], Sourav Maity[a], Shewli Pratihar[a], Shrabanee Sen[a,*]

[a]Functional Materials and Devices Division (FMDD), CSIR-Central Glass & Ceramic Research Institute (CSIR-CGCRI), Kolkata, West Bengal-700032, India

[a]Dipartimento di Fisica, Università della Calabria, Rende- 87036, Italy

*E-mail: shrabanee@cgcri.res.in

Note S1

Optimization of filler concentration

In the experimental condition of the present work, it was difficult to fabricate PVDF based composite films with higher concentration of filler loading than that of 10 wt%. After 10 wt% filler loading, the film started being curly which was not good enough for the triboelectric device fabrication. Furthermore, after 10 wt% of filler loading, the overall polar phase of PVDF based composites and their output piezoelectric energy harvesting performance deteriorated probably due to higher agglomeration of fillers within PVDF. Therefore, in order to develop the device with optimized performance, up to 10 wt% filler loading was considered in this work. As the main objective of the present work is to show the effect of polarization tuning on the output performance of the fabricated hybrid device, detail filler concentration dependent study is not shown here.

For PDMS based composites, higher filler concentration compared to that of 10 wt% resulted in the precipitation of filler at the bottom of the composite film which resulted in non-uniform output energy harvesting performance. Therefore, for PDMS based composite also, the filler concentration was restricted up to 10 wt% only.

For both the PVDF and PDMS based composite films, lower filler loading compared to that of 3 wt% did not show much significant effect in improving the dielectric polarization of the composite films. As the key objective of the present work is to show the effect of polarization rationalization, lower filler concentration than that of 3 wt% was therefore not considered. Hence, for both of the composite films, filler loading was restricted within 3-10 wt%.

Note S2

Details about dielectric and *P-E* loop characterization

For dielectric and *P-E* loop characterization of BFO, a bulk pellet of this sample was prepared and both sides of the pellet were electroded with high quality silver paste. The dielectric study was performed under 1 V of bias field and the *P-E* hysteresis loops were recorded under the application of triangular waveform of 1 Hz frequency.

In this regard, it is to be mentioned that, the BFO filler interact with macromolecules of the polymers via particle-polymer interaction. Thus, in order to perfectly describe the electrical characterization of the fabricated composite systems, dielectric permittivity and *P-E* loop of

BFO nanoparticles and macromolecules of polymers are needed to be investigated which could not be performed in the present work due to lack of facilities. Here we could only study the electrical parameters of the filler material and polymer based composites in bulk form. The dielectric permittivity of bulk BFO pellet was found to be much higher compared to that of the neat polymer materials (in bulk film form). Thus, for the sake of simplicity, the BFO nanoparticles were consider to exhibit higher value of dielectric permittivity compared to that of the polymer macromolecules. This type of consideration is often made by the researchers all over the world.[21-22,37,S1-S2] Therefore, it has been considered that the inclusion of BFO nanoparticles in polymer matrix will improve the dielectric polarization of the resulting composite system which is also confirmed from our experimental results of dielectric permittivity of BFO-PVDF and BFO-PDMS composite systems.

Fig. S1

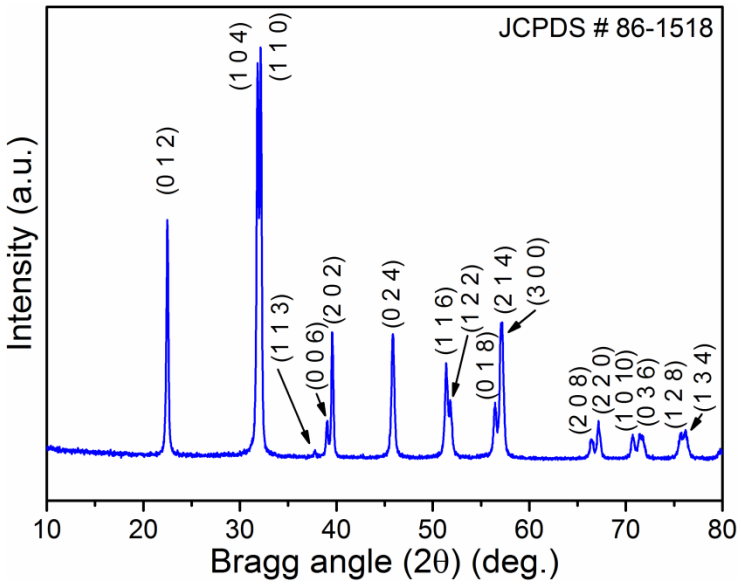

Fig. S1 Indexed XRD pattern of BFO nanoparticles.

Table S1

Table S1 Refined lattice parameters and structure fitting factors of XRD pattern of BFO.

Sample and its space-group	Lattice Parameters	Atoms	Atomic positions (x, y, z)	Fitting factors
BFO (R3c)	a = 5.5763Å c = 13.8648Å V = 373.375$Å^3$	Bi Fe O	0, 0, 0 0, 0, 0.2231 0.4347, -0.0224, 0.9513	R_p= 17.5% R_{wp}= 18.7% $\chi^2 = 1.88$

Fig. S2

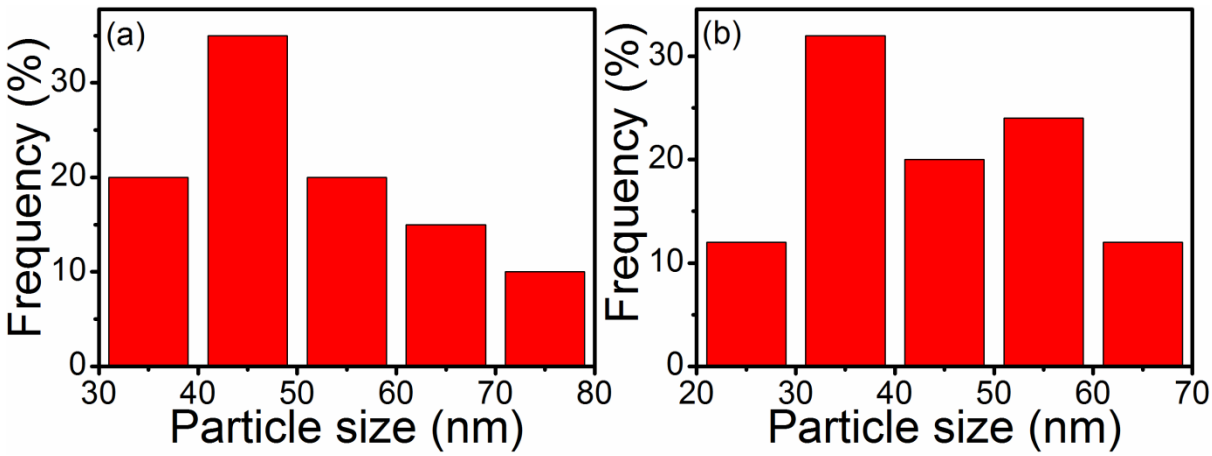

Fig. S2 Size distribution of the synthesized BFO nanoparticles from (a) FESEM and (b) TEM images, respectively. [Only those particles were taken for the calculation of size distribution, which were able to be clearly distinguished. The average particle from FESEM and TEM was found to be ~ 50 nm and ~ 48 nm, respectively. As the FESEM image exhibits much agglomerating nature, the average size from TEM was selected as the correct one. However, both the FESEM and TEM image showed almost same average particle size.]

Fig. S3

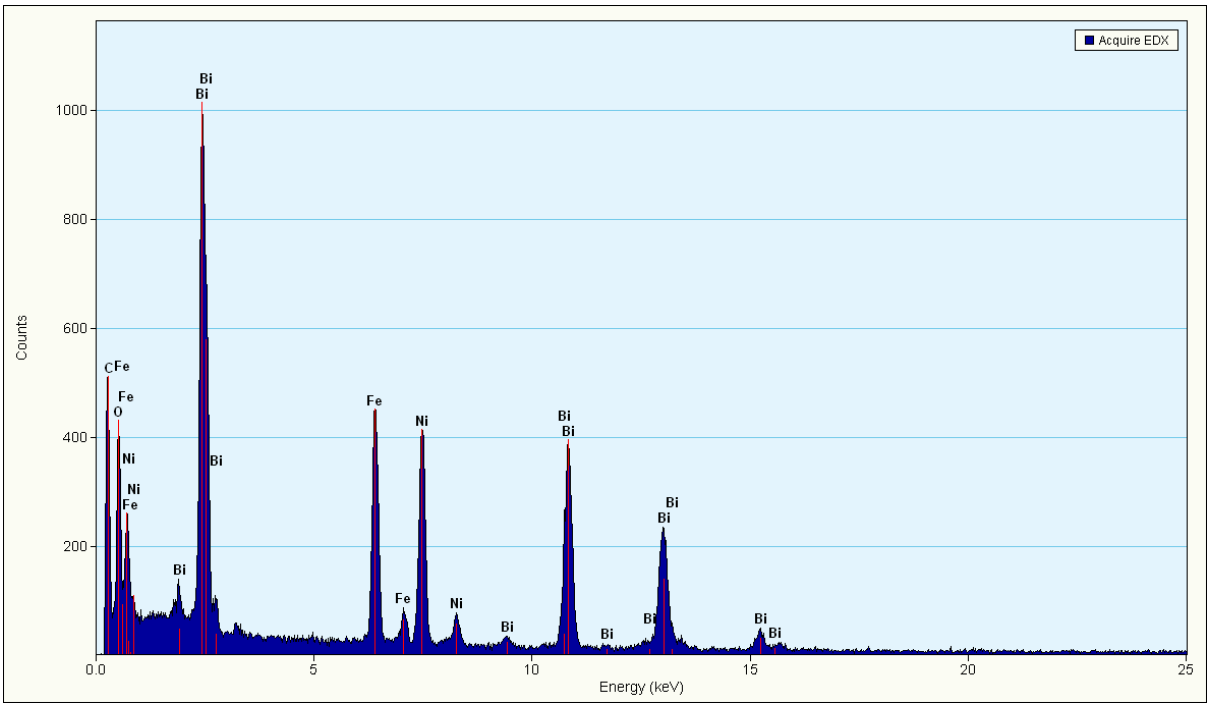

Fig. S3 EDX spectra of synthesized BFO nanoparticles (signal of Ni appeared from the Nickel grid) reported in our previous work.[35]

Fig. S4

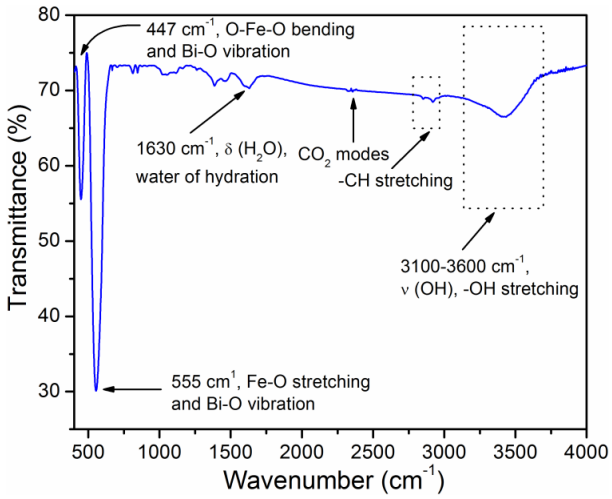

Fig. S4 FTIR transmission spectra of the synthesized BFO with indexing of vibrational bands.

Note S3

Analysis of *P-E* hysteresis loop of BFO

During *P-E* loop characterization of BFO pellet, a maximum of ~ 6 kV/cm electric field could be applied. After that, the breakdown of the sample occurred. But, the reported value of coercive field of BFO is very high (~ 50 kV/cm)[48-49] compared to the maximum applied field in the present work. Therefore, though BFO is known to show ferroelectric properties, the occurrence of hysteresis in the *P-E* loop (Fig. 2(h)) for the low applied field in the present work confirms the fact that, the hysteresis is governed by the conductive nature of the sample.[50] Thus, the perfect ferroelectric nature of BFO can not be estimated from Fig. 2(h). The ferroelectricity of BFO can only be considered into account based on the previously reported literatures. However, the Fig. 2(h) can confirm the conductive nature BFO which is also helpful in enhancing the output performance of the composite film based energy harvesters.

Note S4

Interfacial interaction of BFO surface with PVDF dipoles

BFO exhibits negative surface potential (reported in our previous work)[34] which confirmed its negative surface charge. Therefore $–CH_2$ dipoles of PVDF (exhibiting positive polarity/charge) are commonly attracted toward BFO particle surface. The neat PVDF

composite film predominantly contained the non-polar α phase which after interaction with BFO particle surfaces transformed to polar β and/or γ phase due to re-orientation of dipoles caused by interfacial electrostatic interaction resulting in polar chain conformation.[34] Neat PVDF and all the BFO loaded PVDF films exhibited all the mentioned three phases. But, the amount of polar phase (electroactive phase percentage) was found to be ~ 39% for neat PVDF and 82-89% for 2-7 wt% BFO loaded composite films (reported in our previous work).[35] For 10 wt% BFO loaded PVDF film (10PVDF) this amount was found to be ~ 90% (calculated from Fig. S5). Thus, it was concluded that the gradual increase in BFO concentration in PVDF matrix up to 10 wt% resulted in gradually enhanced polar phase caused by enhanced interfacial interaction. The values of polar phase percentage confirmed that, at ~ 10 wt% filler loading, the amount of polar phase started saturating. After 10 wt% filler loading, the polar phase percentage reduced (not shown here) probably due to the increased agglomeration of BFO in PVDF matrix.[20,S3]

Fig. S5

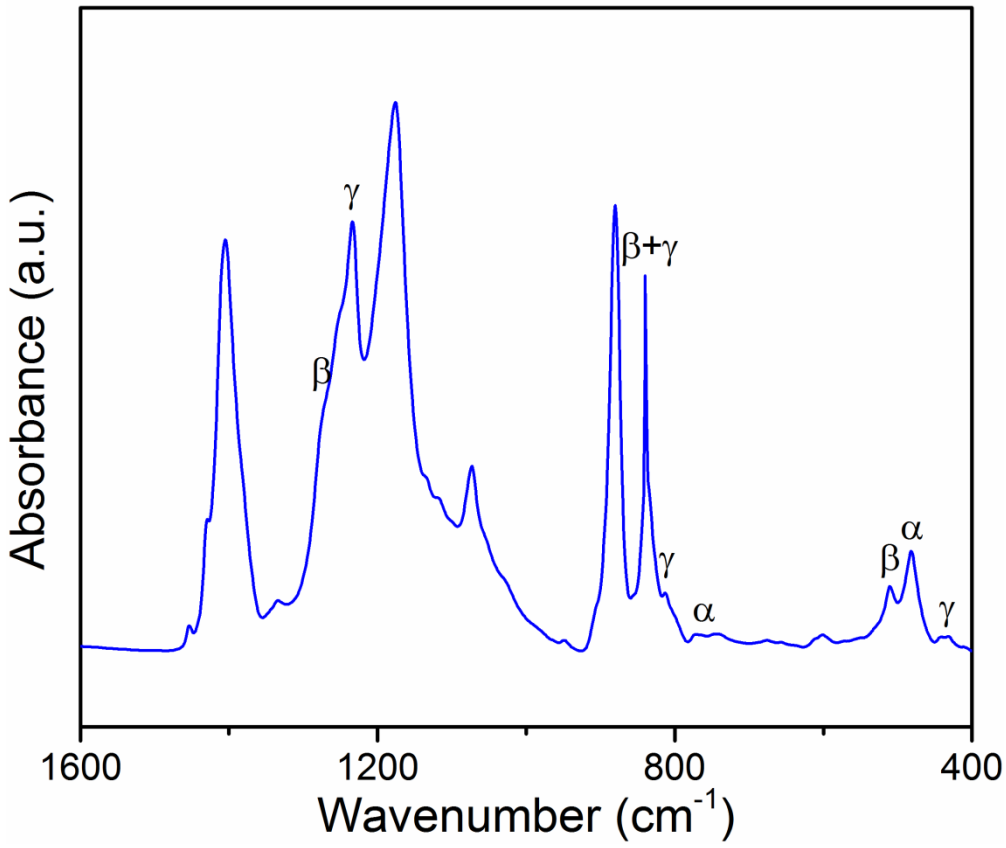

Fig. S5 FTIR absorption spectra of 10 wt% BFO loaded PVDF (10PVDF) composite film within the wavenumber range of 400-1600 cm^{-1}.

Note S5

Working mechanism of piezoelectric nanogenerators

In order to achieve piezoelectric output signal from any piezoelectric material, external electrical poling is a must needed technique for alignment of dipoles. But, in the present work, the piezoelectric output signal from both the PVDF-BFO and PDMS-BFO films was obtained without any external electrical poling. This is directly associated with the stress-induced poling effect.[S4-S6] The generation of the piezoelectric signal from this type of unpoled composite films are very often described on the basis of stress-induced poling effect by the researchers all over the world.[13,S7] The working mechanism of piezoelectric output electrical signal generation from the fabricated PVDF-BFO and PDMS-BFO based unpoled piezoelectric nanogenerators is presented in Fig. S6 and briefly described below.

In the initial state (step-a) (Fig. S6(a)), when there is no applied force on the piezoelectric nanogenerators, the dipoles are oriented randomly, resulting in zero dipole moment and no piezoelectric potential. In this regard, it is to be mentioned that, both the PVDF-BFO and PDMS-BFO films contain randomly oriented BFO dipoles and the PVDF-BFO films also exhibit PVDF dipoles (β and/or γ PVDF) resulting from the interfacial interaction between BFO and PVDF. PVDF based films are thus considered to be self-poled by many researchers. However, when there is no applied stress, we consider all the dipoles to be oriented randomly. In the next step (step-b), when a vertical compressive force is applied, piezoelectric potential is generated inside the dipoles abruptly and the dipoles orient themselves in a single direction along the applied force due to high directionality of the dipoles caused by stress induced poling effect.[13,S7] By this process, significant amount of piezoelectric potential is developed across the top and bottom electrodes. To screen this piezoelectric potential, positive and negative charges are accumulated, respectively, in the top and bottom electrodes (Fig. S6(b)). As a result of this fact, output current starts flowing through the external load resistance. Finally, in the next step (step-c) (Fig. S6(c)), when external force is removed, the piezoelectric potential is also diminished and as a result the accumulated charges move back in the opposite direction. By the application of force and its removal, ac type output electrical signal is thus generated. This type of stress induced poling effect is also well-verified by other researchers.[13,S7] Thus, in order to achieve output electrical signal from the fabricated piezoelectric nanogenerator devices, no external electrical poling was applied in the present work. Stress induced poling effect helped the dipole alignment.

Fig. S6

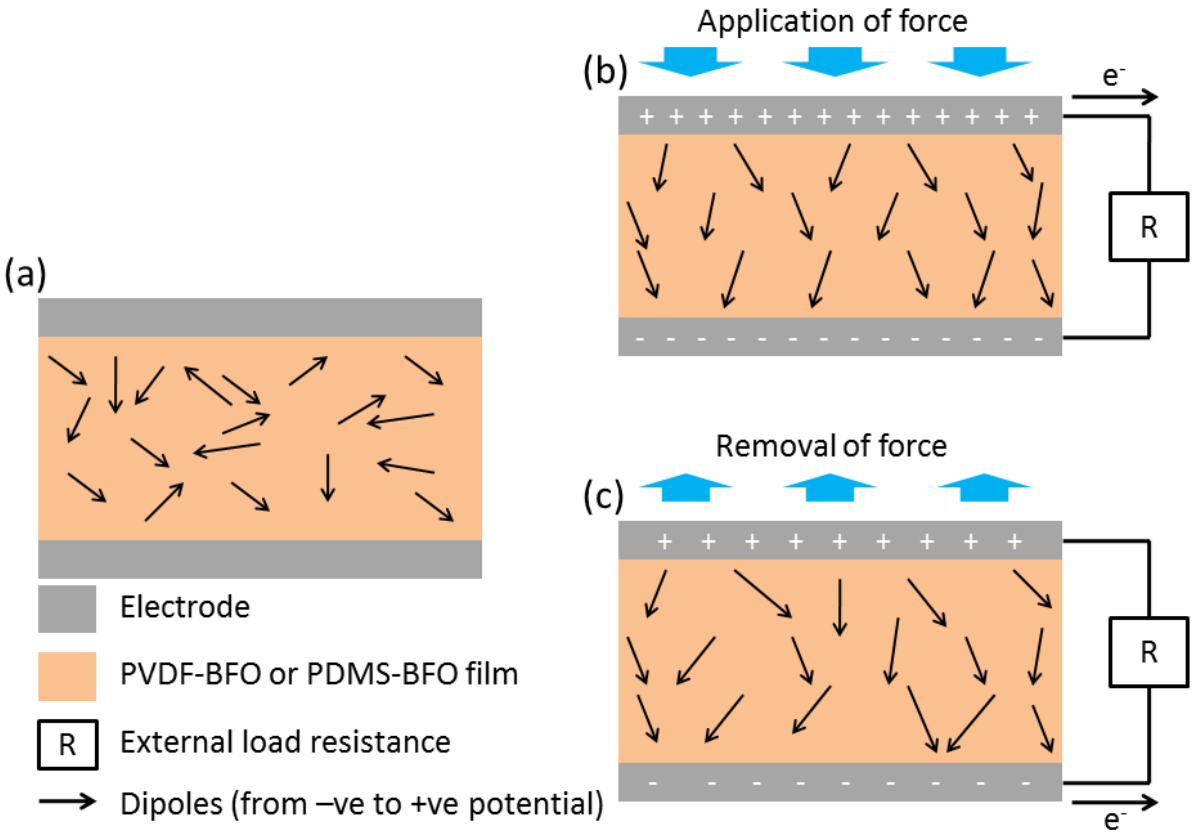

Fig. S6 Working mechanism of piezoelectric nanogenerators.

Movie S1

Movie S1 Glowing of some LEDs connected in series during each tapping on the M-HNG (attached mp4 'Movie' file).

Movie S2

Movie S2 Lighting up of a single LED during each tapping on the M-HNG (attached mp4 'Movie' file).

Fig. S7

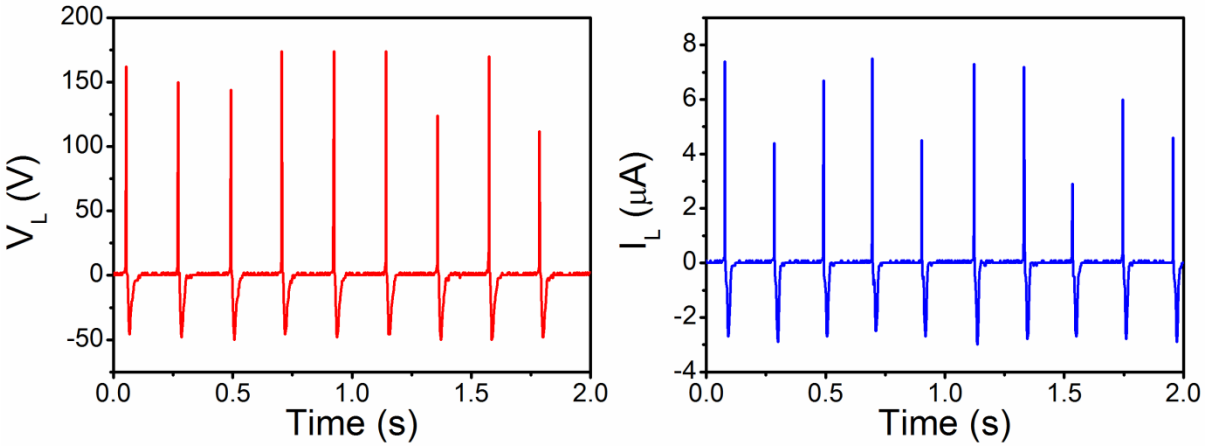

Fig. S7 Output ac V_L and I_L from the M-HNG upon repeated human finger tapping (~ 2 kPa, 5 Hz) on it after placing the device inside an insulated zip-pack.

Fig. S8

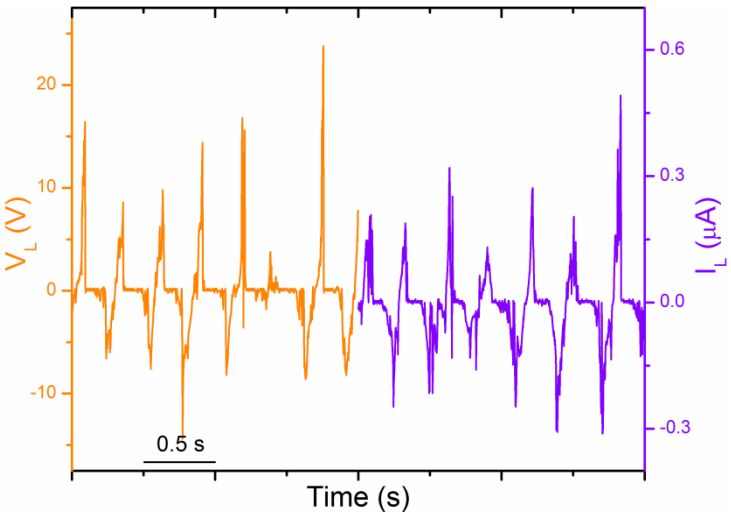

Fig. S8 Energy harvesting from backpack during running condition.

Fig. S9

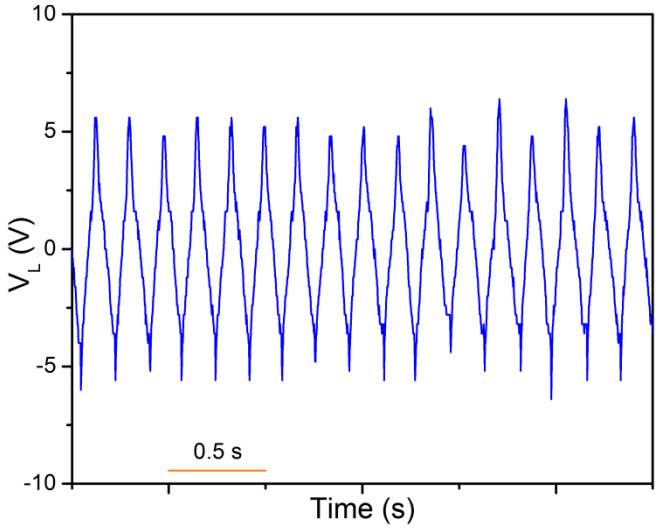

Fig. S9 Output V_L from the M-HNG upon repeated touching without removing the finger from the device.

Fig. S10

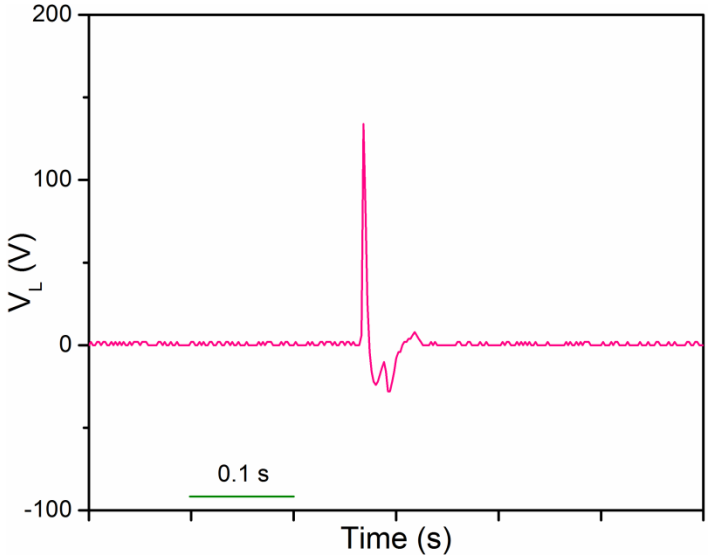

Fig. S10 Output V_L from the device upon ball dropping from 100 cm height on it.

Fig. S11

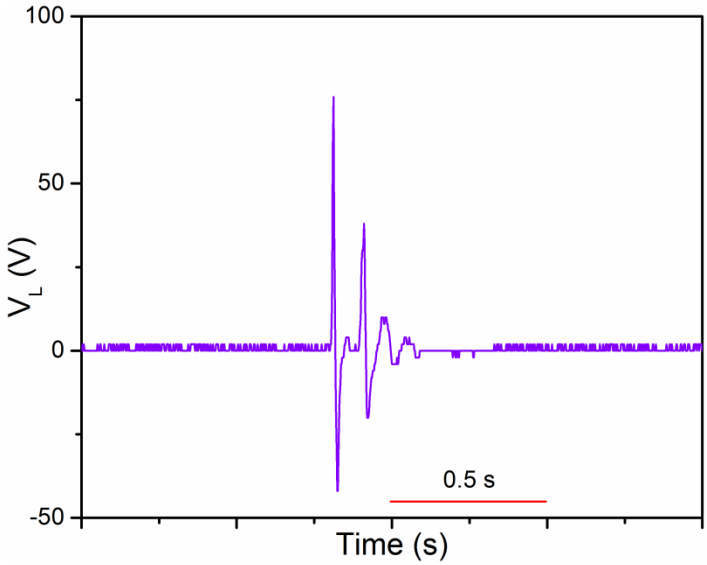

Fig. S11 Output V_L corresponding to dropping and re-bouncing of the ball released from 3 cm height.

Movie S3

Movie S3 Response of the device upon continuous water dropping on it (attached mp4 'Movie' file).

Fig. S12

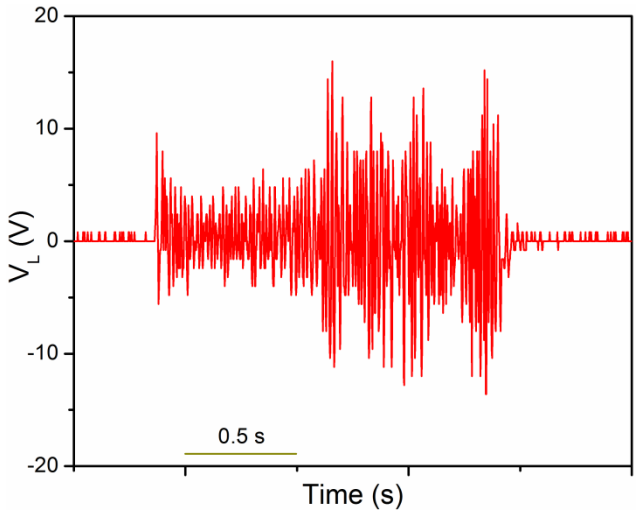

Fig. S12 Output V_L from the device upon normal tap water flow on it.

Fig. S13

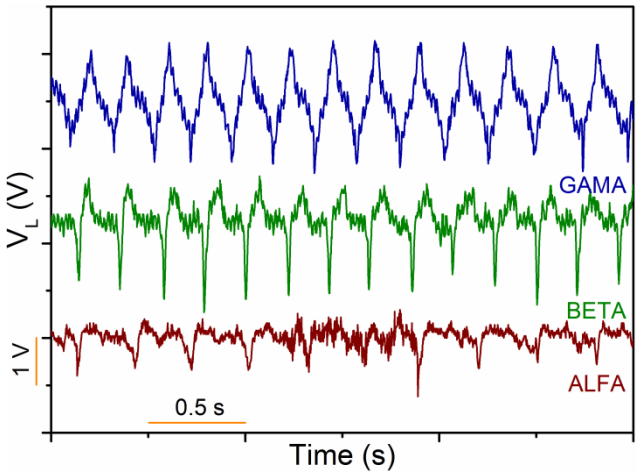

Fig. S13 Output V_L from the M-HNG device during pronunciation of ALFA, BETA and GAMA after attaching the device on the throat of a male participant.

References

S1. S. A. Riquelme, K. Ramam and A. F. Jaramillo, *Results Phys.*, 2019, **15**, 102800.

S2. A. Bele, M. Cazacu, G. Stiubianu, S. Vlad and M. Ignat, *Composites: Part B*, 2015, **68**, 237-245.

S3. J. Liu, B. Yang, L. Liu, X. Wang, X. Li, X. Chen and J. Liu, *Sens. Actuator A Phys.*, 2020, **303**, 111796.

S4. T. Kumazawa, Y. Kumagai, H. Miura, M. Kitano and K. Kushida, *Appl. Phys. Lett.*, 1998, **72**, 608.

S5. A. Gruverman, B. J. Rodriguez, A. I. Kingon, R. J. Nemanich, A. K. Tagantsev, J. S. Cross and M. Tsukada, *Appl. Phys. Lett.*, 2003, **83**, 728.

S6. A. G. Luchaninov, A. V. Shilnikov, L. A. Shuvalov and V. A. Malyshev, *Ferroelectrics*, 1993, **145**, 235-239.

S7. C. Zhang, Y. Fan, H. Li, Y. Li, L. Zhang, S. Cao, S. Kuang, Y. Zhao, A. Chen, G. Zhu and Z. L. Wang, *ACS Nano*, 2018, **12**, 4803-4811.